Carbohydrate Polymers 112 (2014) 668–676

Contents lists available at ScienceDirect

Carbohydrate Polymers

journal homepage: www.elsevier.com/locate/carbpol

Nanoporous membranes with cellulose nanocrystals as functional entity in chitosan: Removal of dyes from water

Zoheb Karim [a,b], Aji P. Mathew [a,*], Mattias Grahn [b], Johanne Mouzon [b], Kristiina Oksman [a]

[a] Division of Materials Science, Luleå University of Technology, 97187, Luleå, Sweden
[b] Department of Civil, Environmental and Natural Resources Engineering, Division of Sustainable Process Engineering, 97187, Luleå, Sweden

ARTICLE INFO

Article history:
Received 19 April 2014
Received in revised form 7 June 2014
Accepted 11 June 2014
Available online 25 June 2014

Keywords:
Cellulose nanocrystals
Chitosan
Nanoenabled membranes
Dye removal
Water purification
Adsorption

ABSTRACT

Fully biobased composite membranes for water purification were fabricated with cellulose nanocrystals (CNCs) as functional entities in chitosan matrix via freeze-drying process followed by compacting. The chitosan (10 wt%) bound the CNCs in a stable and nanoporous membrane structure with thickness of 250–270 μm, which was further stabilized by cross-linking with gluteraldehyde vapors. Scanning electron microscopy (SEM) studies revealed well-individualized CNCs embedded in a matrix of chitosan. Brunauer, Emmett and Teller (BET) measurements showed that the membranes were nanoporous with pores in the range of 13–10 nm. In spite of the low water flux (64 L m^{-2} h^{-1}), the membranes successfully removed 98%, 84% and 70% respectively of positively charged dyes like Victoria Blue 2B, Methyl Violet 2B and Rhodamine 6G, after a contact time of 24 h. The removal of dyes was expected to be driven by the electrostatic attraction between negatively charged CNCs and the positively charged dyes.

1. Introduction

Shortage and contamination of global drinking water call for the development of highly effective water purification techniques. The removal of various pollutants such as heavy metals, dyes, pesticides, herbicides and other industrial as well as agricultural wastes from wastewater has become a critical issue due to their adverse effects on human health and environment (Huang, Chang, Ou, Chiang, & Wang, 2011; Lin, Chen, Chien, Chiou, & Liu, 2011)

Recently, advances in nanoscale science and engineering suggest that many of the current problems involving water quality could be greatly diminished by using nanomaterials due to their good adsorption efficiency, higher surface area and greater active sites for interaction with pollutants (Dhermendra, Behari, & Prasenjit, 2008; Diallo, Christie, Swaminathan, Johnson, & Goddard, 2005). Several studies have shown the effectiveness of nanoenabled membranes for cleaning industrial wastewater such as fish-meal wastewater, solutes from etching processes, wastewater from textile industry, etc. (Dhermendra et al., 2008; Ma, Burger, Hsiao, & Chu, 2011a). However these technologies poses significant challenges in term of limited availability of nanomaterials, cost effectiveness and environmental concerns.

Polysaccharides, such as cellulose and chitin, are among the most abundant biomaterials on earth, having low cost, environmental friendly, renewable and biodegradable properties (Muzzarelli, 2012; Muzzarelli et al., 2007; Samir, Alloin, & Dufresne, 2005). By intelligent processing techniques and properties they could be used as classical nano-reinforcements/functional elements in polymers for the preparation of membranes (Ma et al., 2011a; Ma, Burger, Hsiao, & Chu, 2012). Cellulose nanocrystals (CNCs) and nanofibers isolated from bioresources have been studied as reinforcements and/or functional entity in various synthetic and natural polymer matrices and for different applications (Kvein et al., 2007; Mathew, Oksman, Pierron, & Harmand, 2012; Mikkonen et al., 2010; Narges et al., 2014; Petersson, Kvien, & Oksman, 2007; Samir et al., 2005; Saxena, Elder, Pan, & Ragauskas, 2009). Recently, Ma et al. (2012) developed a membrane, where ultrafine CNCs were infused into an electrospun polyacrylonitrile nanofibrous scaffold supported by mechanically strong polyethylene terephthalate non-woven substrate. The impregnated CNCs possessed very high negative surface charge density and thus provided high adsorption capacity to remove positively charged species, viz. crystal violet dye. Thus, adsorption has been proved to be an economical method for the treatment of wastewater contaminants. Now-a-days, almost all the adsorbents developed for removal of contaminants rely on the surface interactions and therefore the functional groups available on the surface of the adsorbents played an important role in determining the effectiveness, capacity,

* Corresponding author. Tel.: +46 92493336.
E-mail address: aji.mathew@ltu.se (A.P. Mathew).

http://dx.doi.org/10.1016/j.carbpol.2014.06.048
0144-8617/

selectivity and reusability of the adsorbent material (Dural, Cavas, Papageorgiou, & Katsaros, 2011; Liu, Wang, & Li, 2005; Wesenberg, Kyriakides, & Agathos, 2003; Xiao et al., 2010). Furthermore large surface area and abundance of adsorption sites are essential for adsorption and removal of the contaminants from wastewater (Li & Bai, 2005; Li, Bai, & Liu, 2005; Liu et al., 2014).

In the current study CNCs having required functional groups (SO^{3-} and/or COO^{-}) (Liu et al., 2014) for the removal of targeted dyes by electrostatic interaction, are used as functional entity for the fabrication of composite membranes. Chitosan is used as the matrix phase. Though chitosan is traditionally used in water purification, it is mostly effective toward negatively charged acidic dyes due to functional group present on chitosan ($-NH_2^+$) (Bingjie, Dongfeng, Guangli, & Xianghong, 2013; Crini, 2006). However, the water permeability and water stability of chitosan in different pH conditions, especially after cross-linking will be of advantage in fabricating water-cleaning membranes (Mathew, Laborie, & Oksman, 2009). A very simple technique, freeze-drying was applied for the fabrication of composite membranes. The biggest advantage with process was fabrication of a loose and non-aggregated network, which is expected to provide easy availability of surface groups on CNCs as adsorption sites for contaminants. High concentration of functional entity (CNCs) was used with an aim to have high process efficiency. The process method as well the matrix used is expected to make the surfaces of functional entity readily available for interaction with contaminants in water.

ATR-FTIR analysis was performed to understand the basic binding parameters with CNCs and matrix, chitosan. SEM and BET techniques were used to characterize the membrane morphology and pore structure. Flux and mechanical performance of the composite membranes were also determined. Three positively charged dyes (Victoria Blue 2B, Methyl Violet 2B and Rhodamine 6G) that are real concern in industrial wastewater were chosen for the study. It may be noted that these dyes are of industrial and environmental relevance as (i) according to the Swedish Environmental Protection Agency, the selected dyes came under section "very hazardous" contaminants, (ii) the three selected dyes having negative impact in southern Europe, especially in Spain and (iii) these dyes had very harmful effects not only on human but on aquatic life also.

2. Experimental

2.1. Materials

Non-dried cellulose residue (sludge) from dissolving cellulose production was obtained from Domsoj Fabriker AB, Ornskoldsrik Mill, Sweden, with a water content of 50 wt%. Based on the data from the material supplier, the chemical composition of the used sludge was, cellulose content (95%), hemicellulose (4.75%) and very low content of lignin.

Chitosan from shrimp shells (medium molecular weight having deacetylation value ≥75.5% and viscosity, 20–300 cps), polyethylene glycol (PEG 2000) and gluteraldehyde (50%) were purchased from Sigma–Aldrich (USA). Acetic acid (96%) and sulfuric acid (98%) were supplied by VWR (BDH, France).

Sludge was used as received without any pretreatments and all chemicals were used without any purification.

2.2. Processing methods

2.2.1. Isolation and characterization of CNCs

CNCs were prepared by acid hydrolysis of non-dried cellulose residue (sludge) following the sulfuric acid hydrolysis as procedure by Bondeson, Mathew, and Oksman (2006), with minor modifications. The sludge was hydrolyzed with 63.5% sulfuric acid for 105 min at 45 °C. The resulting suspension underwent a series of centrifugation, washing with deionized water, and sonication steps to collect the CNCs in the supernatant. This was neutralized by dialysis and stored until further use in the form of aqueous suspensions. Isolated CNCs were concentrated by dialysis against PEG to a concentration of 4.2 wt% prior to use for membrane fabrication. The yield of CNCs from the process was 17% with respect to the used cellulose residue weight.

2.2.2. Preparation and cross-linking of nanocomposite membrane

Chitosan was first dissolved in 2 wt% acetic acid followed by addition of deionized water to form a solution of 1 wt%. The concentrated CNCs were mixed with chitosan solution in 9:1 ratios and the total concentration of mix was 2 wt%. The mixture of chitosan and CNCs were casted into Petri plates and put into freezer to solidify. The solidified mixture was freeze-dried in an ALPHA 2-4 LD Plus freeze dryer at −75 °C for 24 h. After freeze-drying, the prepared porous composites were pressed between aluminum plates in a compression molding machine (Fontune Presses, Elastocon, Sweden) without heating to obtain compacted membranes. Same procedure was followed for the preparation of native chitosan (0.2 wt%), used as control. Cross-linking was performed by placing the compacted membranes in a desiccator with gluteraldehyde vapors; 25% of gluteraldehyde at room temperature for 48 h was used. In uncross-linked as well as cross-linked membranes the final CNC concentration was 90 wt%.

2.3. Characterizations

2.3.1. Morphology and pore structure

Atomic force microscopy (AFM) was analyzed using a Veeco Multi Mode instrument equipped with Nanoscope V controller. A droplet of the aqueous CNCs suspension (0.2%) was dried on a freshly cleaved mica surface prior to AFM examination. AFM images were captured in tapping mode using coated Si probes at a resonance frequency of 70 kHz and having a spring constant of 1–5 N/m.

The morphology of uncross-linked and cross-linked membranes was examined at high magnification using MAGELLAN 400, SEM (FEI Company). The membranes were fractured and sputter coated with tungsten. The films were observed in the SEM at an acceleration voltage of 20 kV.

2.3.2. Chemical characteristics

A Bruker IFS 66v/S spectrometer equipped with liquid nitrogen cooled mercury–cadmium–telluride (MCT) detector and a vertical ATR-FTIR accessory was used for collecting infrared data. Both single beam background and sample spectra were acquired by averaging 500 scans at a resolution of 4 cm^{-1}. Spectra evaluation was performed using the Bruker Opus 4.2 software.

2.3.3. Porosity

Specific surface area and pore size of fabricated composites were determined by N_2 adsorption using BET method with sample-degassed instrument (Micromeritics ASAP 2000, Sweden) at 100 °C for 24 h in dry N_2 flow.

2.3.4. Mechanical properties

The tensile tests of the uncross-linked and cross-linked membranes were performed using a universal testing machine, Shimadzu Autograph AG-X (Japan), with a load cell 1 kN and the gauge length was 20 mm. Test specimens were 5 mm and 0.25 mm in nominal width and thickness as measured by digital caliper for membrane. The samples were preloaded with 1 N before starting the tensile test. The samples were stretched with 2 mm/min crosshead speed until failure. The stress–strain curves were plotted from the measured load and samples extension. The stress is

defined as $\sigma = F/(A_0 L_0)$ and the strain as $\varepsilon = \ln(L/L_0)$, where F is the instantaneous force, A_0 is the initial sample cross section, and L_0 is the initial sample length. The elastic modulus was calculated from the initial part of the slope from the stress–strain curve. At least five test samples were tested for each material and the average values were presented.

2.3.5. Flux measurement

A dead-end stirred cell filtration system connected with a N_2 gas cylinder was used to evaluate the flux performance of the composite membranes. All experiments were carried out using a filtration test cell, Dead End Cell (Sterlitech HP4750 Stirred cell, USA) with a capacity of 300 ml. The effective area of the membrane was 17.3 cm^2. The operation pressure (0.196 MPa) in the system was maintained by nitrogen gas. Composite membranes were conditioned in water for 1 day prior to measurement of water flux. The amount of solvent passing through the membranes under applied pressure within a fixed time interval was used to calculate water flux (L m^{-2} h^{-1} MPa^{-1}). The water flux (F) was calculated using Eq. (1).

$$F = \frac{V_0\,(\mathrm{L})}{T_0\,(\mathrm{h})} \times A_0\,(\mathrm{m}^2) \times P_0\,(\mathrm{MPa}) \quad (1)$$

where V_0 is the volume of solvent that passed through the membrane, T_0 is the time of measurement, A_0 is the effective membrane area and P_0 is the applied pressure.

It was not possible to measure the water flux of pure chitosan as the freeze-dried structure was completely destroyed because of dipping chitosan membrane in water before measurement of water flux.

2.3.6. Evaluation of dye removal efficiency

The quantitative analysis of untreated and treated model wastewater was determined by UV–vis spectrophotometer (Perkin Elmer, Lambda 2S, Sweden). The percentage removal was calculated by the formula given below:

$$A_0 - \frac{A_t}{A_0} \times 100 \quad (2)$$

where A_0 is the absorbance of treated dye solution with chitosan membrane and A_t is the absorbance of treated dye solution with composite membrane. The absorbance of each dye was recorded at their λ_{max}, determined by UV–vis spectrophotometer. The optical absorbance of dyes, Methyl Violet 2B, Rhodamine 6G and Victoria Blue 2B at 581, 526 and 616 nm respectively was monitored by UV–vis spectroscopy to determine the percentage removal of dyes. Table 1 summarizes the chemical structure and other parameters of the used dyes.

Some screening experiments on the effect of pH, incubation time and doses of dyes with uncross-linked hybrid membrane only, were performed to determine the best conditions to study the maximum removal efficiency of the prepared hybrid membranes.

Stock solution of model wastewater was prepared by adding dyes (10 mg/L) in deionized water. The 1 mg/L of model wastewater was used with uncross-linked and cross-linked membranes. Composite membranes cut into 30 × 20 mm of pieces were incubated for 24 h in solution of pH 5.01 at room temperature (23 ± 2) with

Table 1
Information about targeted dyes.

Name of dyes	Core structure of dyes	Nomenclature in text	λ_{max}	Charge on surface
Methyl Violet 2B	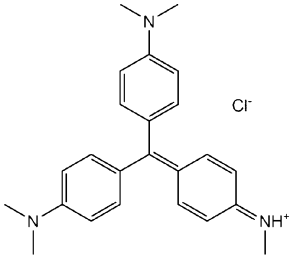	MV 2B	581 nm	+
Rhodamine 6G	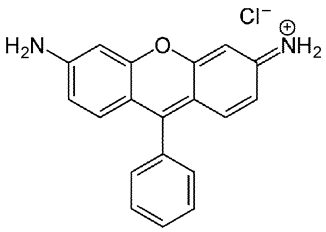	R6G	526 nm	+
Victoria Blue 2B	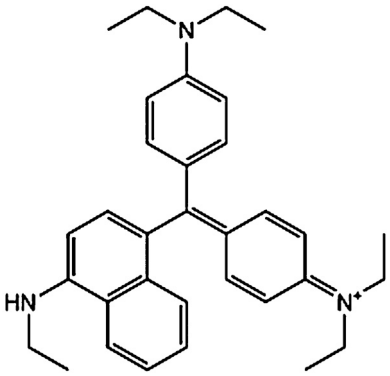	VB 2B	616 nm	+

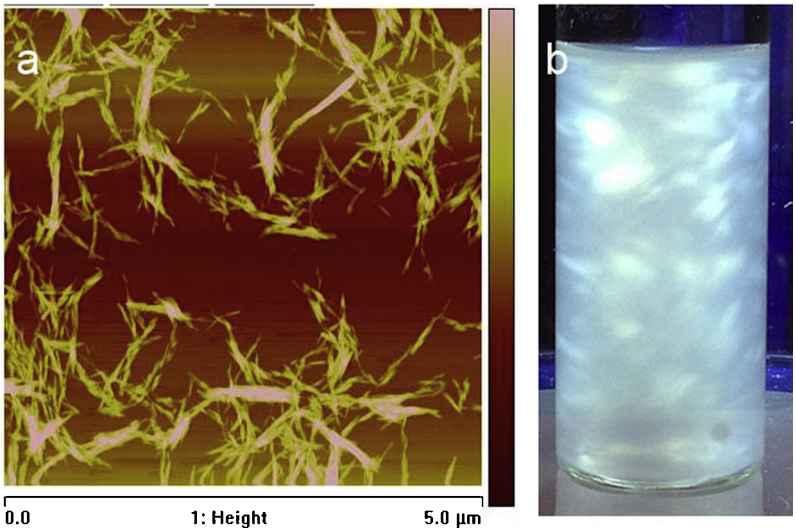

Fig. 1. (a) AFM image of isolated CNCs and (b) flow birefringence of CNCs suspension, observed between two crossed polarizers.

stirring. The model wastewater treated with 0.2% chitosan was taken as control for determination of percentage removal by composite membranes using formula mentioned above. All experiments were performed in dark to prevent the photo-degradation.

3. Results and discussion

3.1. Characteristics of cellulose nanocrystals

The AFM images in Fig. 1 show the presence of isolated cellulose nanocrystals in the nanometer scale. CNC displays rod-like shape with diameters in the range of 6–10 nm, as measured by Nanoscope V software. The nanocrystal dimension agrees with our earlier reports of CNC prepared with same isolation process, by Kvien, Tanem, and Oksman (2005) to be of 5 ± 2 nm width and length of 210 ± 75 nm. The flow birefringence (Fig. 1b) of aqueous nanocrystals when viewed under cross-polarized light also supported the existence of CNCs (Araki, Wada, Kuga, & Okani, 2000; Bondeson et al., 2006).

Crystallinity of isolated CNCs was 70%, and had a surface charge density of 230 μmol/g as calculated from the conductometric titration curve. The *Z*-potential of CNCs remained negative in the pH range of 3–12, as reported in our previous published work (Liu et al., 2014).

3.2. Morphology of prepared composite membrane

Fig. 2a and c shows the overview images for uncross-linked and cross-linked nanocomposite membranes, respectively. The thickness of the membrane was estimated to be in the range of 250–270 μm. In both cases layered structure was observed, which is expected to have formed during compacting of freeze-dried material. Another reason is the high concentration of used CNCs. Recently, Han et al. (2013) reported the concentration dependent mechanism for lamellar or fiber structure morphology of nanocellulose through freeze-drying. According to their results, at low concentration (0.05 wt%), nanocelluloses were self-assembled into oriented ultrafine fibers but at high concentration (0.5 and 1 wt%), the lamellar structured foam composed of aligned thin membrane layers. Similar layered structures were reported for freeze-dried membranes from nanocellulose fibers also (Gebald, Wurzbacher, Tingaut, Zimmermann, & Steinfeld, 2011). The images also show that the cross-linked system is slightly denser than the uncross-linked ones.

Fig. 2b and d shows the detailed view of the uncross-linked and cross-linked nanocomposite membranes. The detailed image shows the nanoscaled morphology of the membranes while the inset image shows one layer of the membranes. The SEM images of uncross-linked membranes showed that CNCs were regularly dispersed within the chitosan forming a network of CNCs with absence of visible agglomerates (Fig. 2b). Cross-linked nanocomposite membrane also shows uniform dispersion of CNCs within the chitosan network in random orientation but little tight network due to the cross-linking with gluteraldehyde (Fig. 2d). The good dispersion of CNCs in chitosan matrix even at high concentration indicates positive interaction between chitosan matrix and CNCs. It may be considered that the CNCs are bound together in a three dimensional network by chitosan chains. In the current study also we have the advantage of the common solvent and furthermore the processing methods used, viz. freeze-drying is considered as an efficient route to limit aggregation of nanocellulose.

Gebald et al. (2011) recently reported cellulose nanofibers membrane for the adsorption of CO_2 prepared by freeze-drying. In this study, SEM images of prepared membrane revealed single irregularly distributed cellulose fibrils attached to the cellulose sheet, after freeze-drying and aggregation of cellulose nanofibrils to form sheet upon freezing was recorded. It is expected that in the current study the combination of the choice of matrix, and the processing method have positively impacted the homogeneous dispersion and distribution of CNCs. The infused and well-dispersed CNCs within the chitosan network offer several advantages in membrane technology as high surface-to-volume ratio that makes them high adsorption efficiency toward contaminants.

3.3. Evaluation of molecular level interactions

To understand the interaction between the chitosan polymer and CNCs in the composite membrane, FTIR spectroscopy of the samples was performed using the ATR (attenuated total reflection) technique (see supplementary data for the spectrum). The spectra of chitosan and CNCs were typical to spectra previously reported on these substances (Pavia, Lampman, & Kriz, 2002), The main bands in the spectrum of chitosan were located around 1643 and 1558 cm^{-1}. The first band was for C=O stretching of acetyl group and the second band was the N—H bending vibrations of amide and amine groups. The bands at 1070 cm^{-1} and 1030 cm^{-1} were due to the C—O stretching vibration, whereas the broad band at 3100–3400 cm^{-1} was on behalf of O—H and N—H stretching

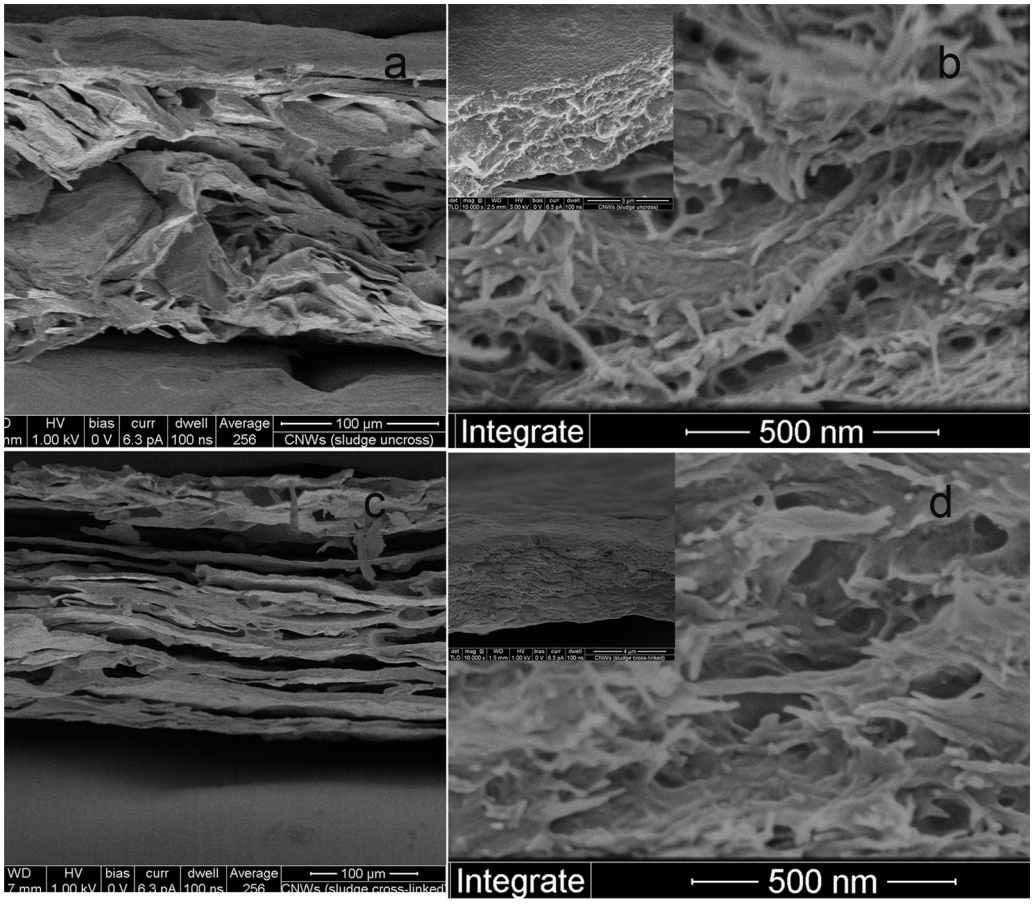

Fig. 2. SEM images of prepared membranes showing (a) layered structure of uncross-linked membranes; (b) the detailed view of the membrane showing the homogeneous dispersion of CNCs in the matrix; c) the layered structure of cross-linked membranes; (d) the detailed view of the CNCs dispersed in the cross-linked matrix. In inset images show one layer of the uncross-linked membrane (inset b) and cross-linked membrane (inset d), comparing the compactness before and after cross-linking.

vibrations. The peaks 1375 cm^{-1} and 1350 cm^{-1} were indicating $-CH_3$ group of *N*-acetyl glucosamine residue and $-CH_2$ groups, respectively. All mentioned peaks were in the agreement of previous reported works. (Brown, Laborie, & Zhang, 2011; Shigemasa, Matsuura, Sashiwa, & Saimoto, 1996).

In pure CNCs, the broad band centered at ca 3400 cm^{-1} was related to O—H stretching vibration. The bands at 2893 cm^{-1} and 1431 cm^{-1} were characteristic of C—H stretching and bending of $-CH_2$ groups, respectively, where the peaks at 1160 cm^{-1} and 1070 cm^{-1} were typical to the saccharide structure as mentioned and summarized by Strand, Sauperl, and Fras-Zemljic (2010).

The spectrum of nanocomposite membrane shows characteristic bands of both raw materials (CNCs and chitosan). The saccharide and the C—H stretching bands at 1160 cm^{-1} and 1070 cm^{-1} in CNC could be observed in the spectrum of the nanocomposite membrane as well as bands related chitosan viz. the C=O stretching and N—H bending bands at 1643 $cm^{-1}$and 1558 cm^{-1}, respectively. Given the structure of chitosan and CNCs and the processing method used, the formation of hydrogen bonds between these compounds is less expected. Both electrostatic and dispersion forces may however also play a part in keeping the composite membranes together. In the case of cross-linked nanocomposite membrane, a relatively weak characteristic absorption band 1550–1600 cm^{-1} can be assigned to the Schiff base (Brown et al., 2011).

It is expected that similarities between the chemical and molecular structures of CNCs and chitosan enable high affinity between both polymers. Generally, CNCs–chitosan intermolecular interaction are based on H-bond, van der Waals forces, ionic and/or covalent bonds, depending on the processing route (Al-Ghouti et al., 2010). In this study, the process of hybrid membrane fabrication was freeze-drying which was directly responsible for the absence of hydrogen bonding, resulting loose network between CNCs and matrix, chitosan. Thus, the bonding between functional entity, CNCs and matrix, chitosan was predominantly by electrostatic interaction, dispersive forces and chemical bonds. The isolation of CNCs with acid hydrolysis (H_2SO_4) introduced sulfate groups (replaced by aldehyde) onto the surface of CNCs. So there was a high chance for introduction of electrostatic interaction within the CNCs and chitosan. According to Strand et al. (2010), the binding of cellulose on chitosan depends only on two factors; (i) a satisfactory amount of anchoring sites especially, introduction of functional groups in/on cellulose, onto which chitosan could bind and at the same time (ii) satisfactory free amino groups of chitosan, and both these binding mechanisms are applicable in the current system.

3.4. Measurement of pore size and surface area of composite membrane

The BET results were summarized in Table 2. The BET surface areas of uncross-linked and cross-linked composite membranes

Table 2
BET results of uncross-linked and cross-linked membranes.

Type	BET surface area (m^2/g)	Average pore size (nm)
Uncross-linked membrane	3.1	17
Cross-linked membrane	2.9	13

Table 3
Mechanical testing results of uncross-linked and cross-linked composite membranes.

Types of membranes	Max stress (MPa)	Strain at break (%)	Modulus of elasticity (MPa)
Uncross-linked	0.98 ± 0.4	0.28 ± 0.4	128 ± 0.6
Cross-linked	1.1 ± 0.3	0.23 ± 0.5	318 ± 0.4

were 3.1 and 2.9 m^2/g, respectively. This surface area is lower than some earlier reports on freeze-dried nanocellulose membrane structures. The freeze-dried NFC showed a BET surface area of 26.8 m^2/g whereas the amine functionalized NFC showed 7.1 m^2/g (Gebald et al., 2011). In the current freeze-dried structures, the compacting process was considered to be responsible for the relatively lower surface area, recorded in BET measurements. The pore sizes of membranes were also determined by same technique and were found to be 17 and 13 nm for uncross-linked and cross-linked composite films, respectively. From these results it was confirmed that the cross-linking decreases surface area as well as pore size of nano-enabled membrane and thereby can be considered as more compacted than the uncross-linked one. This data also supports the SEM observations. The decrease of pore size was also reported by Gebald et al. (2011) when amine was loaded in composite membrane. Recently, Ma et al. (Ma, Burher, Hsiao, & Chu, 2011b; Ma et al., 2012) showed that pore size of CNCs nano-enabled membrane decreased with increased concentration of functional materials.

3.5. Mechanical stability

The mechanical properties of uncross-linked and cross-linked nanocomposites were summarized in Table 3.

The tensile strength of the uncross-linked membrane was 0.98 MPa whereas that of cross-linked ones was 1.1 MPa. The modulus values increased from 128 MPa to 318 MPa after cross-linking. The strain at break showed no difference before and after cross-linking. The low mechanical performance is attributed to the fabrication method used viz. freeze-drying, that restricts the hydrogen bonding between CNCs as well as with the matrix phase and thereby resulting in a loosely bound structure. This processing method used is therefore not the best option in terms of mechanical performance but is good for having well dispersed nanoparticles and a porous structure. Furthermore, the positive impact of cross-linking on mechanical properties was significant especially with respect to modulus of elasticity.

3.6. Flux measurement of composite membranes

The permeability of pure water through the composite nanostructured membrane was 64 $L\,m^{-2}\,h^{-1}\,MPa^{-1}$. The flux values of tested membrane first decreased slowly during the filtration process because of the scaffold compaction. It was found that the stable permeation flux of composite membrane was reached after 1 h of operation. Ma et al. (2011a) had reported that the flux through a microfiltration membrane using CNCs as infused entity within PAN nanofibrous scaffold was 59 $L\,m^{-2}\,h^{-1}\,kPa^{-1}$ and much higher than commercial membrane, GS0.22 (25 $L\,m^{-2}\,h^{-1}\,kPa^{-1}$). The freeze-dried nanocomposite membranes presented in the current work showed lower water permeation flux as compared to both reported membranes, probably due to the high membrane thickness (250–270 μm). However, in the current case low flux is not considered as a disadvantage as increased contact time favors adsorption.

Table 4
Effect of dose of dyes on the removal of dyes.

Doses of dyes (mg/L)	Removal %		
	Methyl Violet 2B	Rhodamine 6G	Victoria Blue 2B
1	91 ± 1.7	70 ± 2.1	98 ± 1.2
5	60 ± 2.3	31 ± 1.9	95 ± 1.3
10	48 ± 1.4	13 ± 1.1	88 ± 1.7

Composite membranes were of 30 × 20 mm in size, standardized values of pH and incubation time were used.

3.7. Dyes removal

The pH conditions, time of incubation and the pollutant concentrations are considered as important parameters that affect the efficiency of dye adsorption. The effect of pH on the percentage of dyes removal from aqueous model wastewater by composite membranes is illustrated in Fig. 3.

Effect of pH was determined by incubation of hybrid composite membranes for 24 h with dyes solutions (1 mg/L) having pHs 5.01, 7.02 and 9.02 at room temperature. In these experiments, the initial solution pH was adjusted to the desired value (pH value 5–9) using either 1 M HCl or 1 M NaOH solutions. Variation in pH can affect the surface charge potential of the adsorbent and degree of ionization. As the surface charge potential decreases with an increase in the solution pH, the electrostatic attraction between positively charged dyes and the surface of adsorbent (composite membrane) is lowered, which may result in an decrease in the rate of adsorption. Fig. 3 shows the maximum percentage removal of dyes from model wastewater at pH 5.01 and the removal percentage decreases with the increase in pH values. The negative zeta-potential of CNC and its dependence on pH was reported in our earlier study (Liu et al., 2014). The functionality of the membranes showed a direct dependence on the zeta-potential of CNC suggesting that surface characteristics of CNC determine the efficiency of adsorption.

The optimum value of pH was chosen as 5.01 and used in the study of the effect of incubation time. The incubation times were varied between 12 and 36 h in dyes solutions (1 mg/L, pH 5.01) at room temperature. The results are shown in Fig. 3. Optimal removal efficiency of composite membranes was observed for 24 h of incubation time for all dyes.

The optimal values of incubation time (24 h) for all dyes and pH were further used for the determination of the dyes doses for the experiments. Table 4 shows the adsorption capacity of fabricated composite membrane at different concentrations. The adsorption

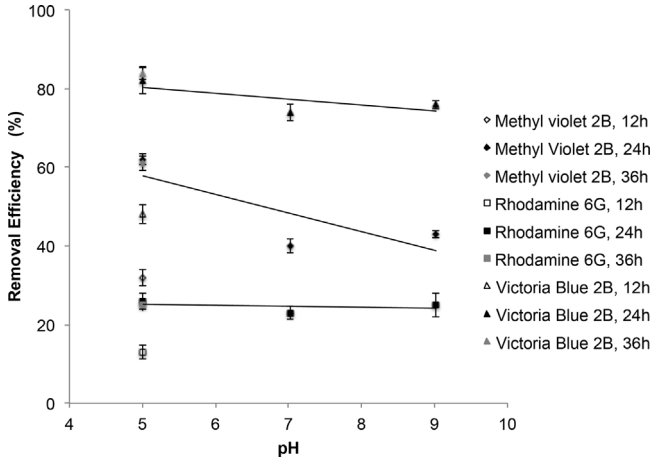

Fig. 3. Graph showing the effect of pH and incubation time on the adsorption of Methyl Violet, Rhodamine 6G and Victoria Blue.

Table 5
Effect of composite membrane on removal of dyes.

Types of dyes	Percentage removal of dyes	
	Uncross-linked membrane	Cross-linked membrane
Methyl Violet 2B	90 ± 2.3	84 ± 1.8
Rhodamine 6G	71 ± 1.6	69 ± 4.2
Victoria Blue 2B	98 ± 3.1	98 ± 3.4

The percentage removal was calculated as mentioned in Eq. (1). The solution treated with 0.2% chitosan membrane was used to measure the value of control.

capacity of composite membrane decreased with increase in the concentration of dyes. Approximately, complete removal (98%) of Victoria Blue 2B was recorded at 1 mg/L concentration. It was inferred that 1 mg/L was the upper limit of dye dosage to evaluate the percentage removal of dyes.

3.8. Removal of dyes with standardized parameters

Targeted dyes having positively charged species were used to determine the adsorption effectiveness of uncross-linked and cross-linked membranes. It was noted that both the membranes were stable in water during the experiments and the cross-linked system showed enhanced dimensional stability which may be attributed to the binding of CNCs in a three dimensional network of chitosan polymer chains. The uncross-linked composites showed slight swelling after contact with dye solutions but were not significant enough to affect the performance.

Table 5 summarizes the dyes removal reached at 24 h by uncross-linked and cross-linked membranes for all dyes solutions. Fig. 4 gives the visual illustration for the removal of dyes by cross-linked composite membranes. It was found that all the dyes showed good adsorption on the membranes being the highest for Victoria Blue followed by Methyl Violet and Rhodamine 6G irrespective of the cross-linking. It is also noted the cross-linking did not have significant impact on the adsorption capability of the membranes. This suggests that the matrix does not influence the adsorption efficiency as it is a minor component (10 wt%) and also due to presence

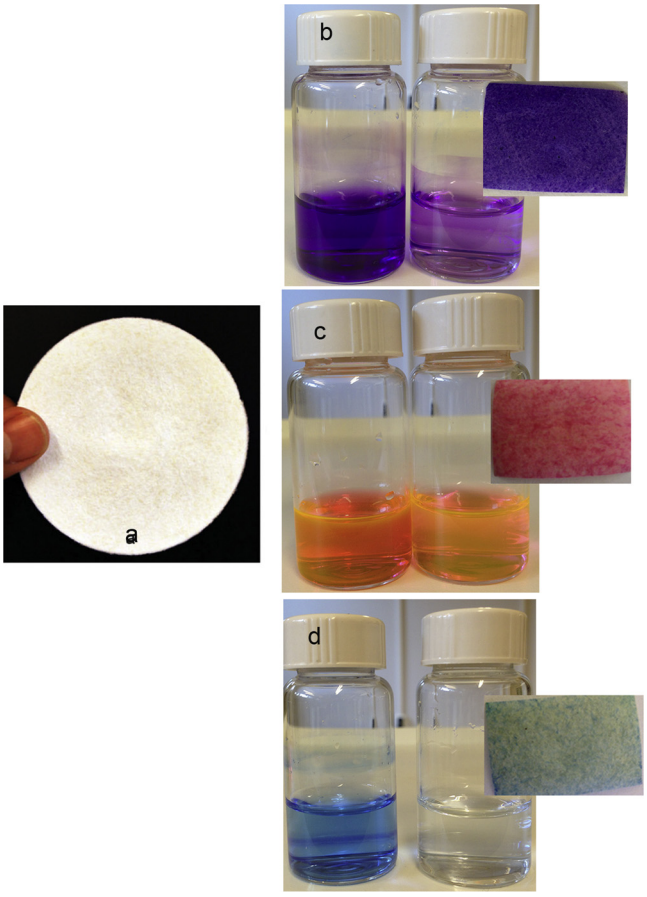

Fig. 4. A schematic representation of experiment shows the naked eyes detection of removal efficiency of cross-linked composite membrane. (a) Photograph of the membrane, water before and after adsorption test for (b) Methyl Violet, (c) Rhodamine 6G and (d) Victoria Blue and the membranes with respective adsorbed dyes.

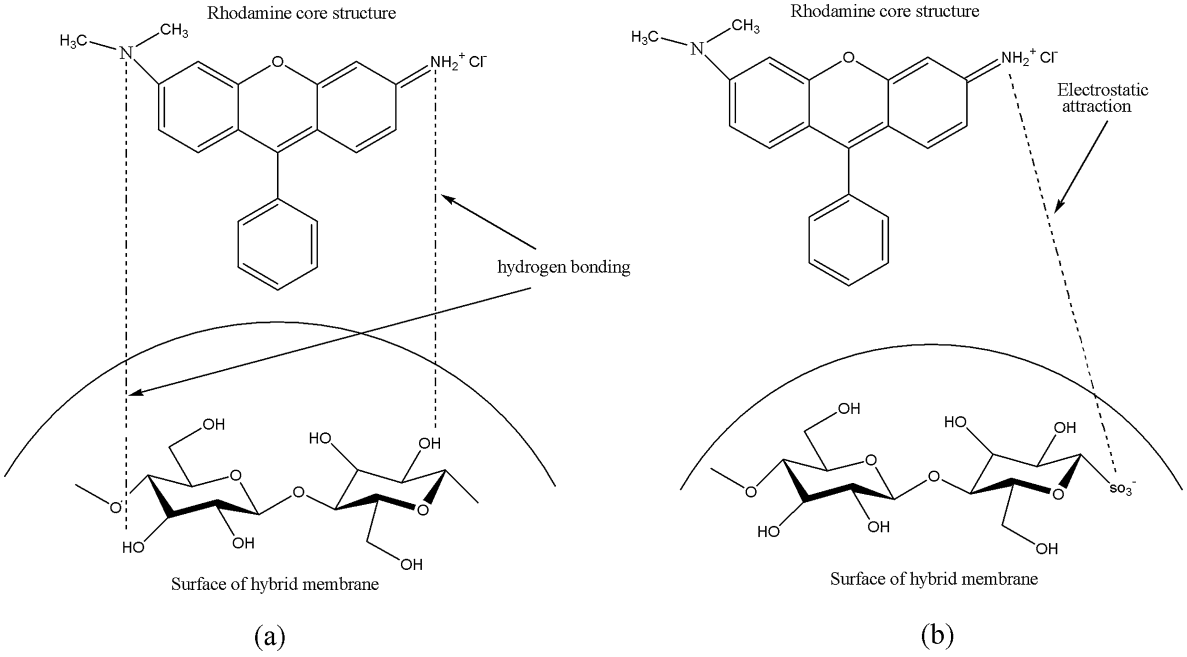

Fig. 5. A schematic representation of the mechanisms of binding of the dyes with CNCs via (a) hydrogen bond formation and (b) electrostatic attraction.

of same charge (positive charge) on surface. This also indicates that the CNCs, which are loosely bound by the matrix are well individualized due to freeze-drying method used and act as the functional entity for capturing the dyes.

The adsorption of dyes may be driven by (i) specific characteristics of dyes (charge, charge potential, functional groups responsible for binding with adsorbent, etc.) and (ii) specific affinity of the dyes for the adsorbent. These kinds of attractions may be predominantly of electrical, van der Waals or chemical nature leading to adsorptions driven by dispersion forces, complexation, hydrogen bond or electrostatic interaction (Al-Ghouti et al., 2010) CNCs with high negative charges on the surface (as confirmed by zeta-potential values) and targeted dyes having positive charges as shown in Table 1, which leads to electrostatic interaction between the pollutants (dyes) and fabricated composite membranes. Fig. 5 further illustrates the electrostatic attraction between dyes molecules and the cellulose-O^- on the membrane surface. Other researchers also in dye removal reported similar mechanisms from water.

Kaewprasit, Hequet, Abidi, and Gourlot (1998) showed the adsorption of methylene blue dye on cotton fiber (cellulose structure) due to the formation of stable ionic bonds between membrane surface and dyes molecules, which prevent dyes molecules from being eluted from the membrane surface. In another study a micro–nano structured poly(ethersulfones)/poly(ethyleneimine) nanofibrous membrane was fabricated and utilized as an adsorbant for three anionic dyes viz., Sunset Yellow, Fast Green and Amaranth (Min et al., 2012). These researchers had further demonstrated that the species of charge present on the surface of composite determined the maximum adsorption of positively charged dye due to the interaction of positive and negative charges.

4. Conclusion

Isolated CNCs isolated from low cost sludge from industrial cellulose production was used as functional entity for the preparation of fully biobased nanocomposite membranes with chitosan as a matrix. Cross-linking of nanocomposite showed positive impact on mechanical stability and dimensional stability in moist environment and also resulted in slight decrease in surface area and pore size. The pore diameter was found to be in 13–17 nm range and classifies these membranes as ultrafiltration membranes. The higher efficiency for the removal of dyes was observed, being the highest for Victoria Blue (98%), followed by Methyl Violet (90%) and Rhodamine 6G (78%). Two mechanisms were proposed for dyes adsorption onto the membrane, hydrogen bonding and electrostatic interaction. Furthermore, the membranes showed low flux ($64\,L\,m^{-2}\,h^{-1}\,MPa$), which supports the usefulness of composite membranes as adsorbents. The high efficiency of the membranes, in terms of adsorption was attributed the freeze-drying process used, which resulted in well individualized CNCs which act as functional entities which were loosely bound together by chitosan polymer chains locked in a 3D network via cross-linking. It may however be noted that freeze-drying adversely affected the mechanical performance of the membranes and will be addressed in the future studies.

Acknowledgements

The authors gratefully acknowledge the financial support by European Commission, under NanoSelect project, EU FP7-NMP4-SL-2012-280519. Iftekhar Uddin Bhuiyan, Luleå University of Technology, is acknowledged for support with BET.

Appendix A. Supplementary data

Supplementary material related to this article can be found, in the online version, at http://dx.doi.org/10.1016/j.carbpol.2014.06.048.

References

Al-Ghouti, M. A., Li, J., Salamh, Y., Al-Laqtah, N., Walker, G., & Ahmad, M. N. M. (2010). Adsorption mechanism of removing heavy metals and dyes from aqueous solution using date pits solid adsorbent. *Journal of Hazardous Materials*, *176*, 510–520.

Araki, J., Wada, M., Kuga, S., & Okani, T. (2000). Birefringent glassy phase of a cellulose microcrystal suspension. *Langmuir*, *16*, 2413–2415.

Bingjie, L., Dongfeng, W., Guangli, Y., & Xianghong, M. (2013). Adsorption of heavy metal ions, dyes and proteins by chitosan composite and derivatives – A review. *Journal of Ocean University of China*, *12*, 500–508.

Bondeson, D., Mathew, A., & Oksman, K. (2006). Optimization of isolation of nanocrystals from microcrystalline cellulose by acid hydrolysis. *Cellulose*, *13*, 171–180.

Brown, E. E., Laborie, M. P., & Zhang, J. (2011). Gluteraldehyde treatment of bacterial cellulose/fibrin composite: Impact on morphology, tensile and viscoelastic properties. *Cellulose*, *4*, 1–11.

Crini, G. (2006). Non-conventional low-cost adsorbents for dye-removal: A review. *Bioresources Technology*, *97*, 1061–1085.

Dhermendra, K. T., Behari, J., & Prasenjit, S. (2008). Application of nanoparticles in wastewater treatment. *World Applied Sciences Journal*, *3*, 417–433.

Diallo, M. S., Christie, S., Swaminathan, P., Johnson, J. H., & Goddard, W. A. (2005). Dendrimer enhanced ultra-filtration recovery of Cu (II) from aqueous solutions using Gx-NH2-PAMAM dendrimers with ethylene diamine core. *Environmental Science and Technology*, *39*, 1366–1377.

Dural, M. U., Cavas, L., Papageorgiou, S. K., & Katsaros, F. K. (2011). Methylene blue adsorption on activated carbon prepared from *Posidonia oceanica* (L.) dead leaves: Kinetics and equilibrium studies. *Chemical Engineering Journal*, *168*, 77–85.

Gebald, C., Wurzbacher, J. A., Tingaut, P., Zimmermann, T., & Steinfeld, A. (2011). Amines-based nanofibrillated cellulose as adsorbent for CO_2 capture. *Environmental Science and Technology*, *45*, 9101–9108.

Huang, C. H., Chang, K. P., Ou, H. D., Chiang, Y. C., & Wang, C. F. (2011). Adsorption of cationic dyes onto mesoporous silica. *Microporous and Mesoporous Materials*, *141*, 102–109.

Han, J., Zhou, C., Wu, Y., Liu, F., & Wu, Q. (2013). Self-Assembling behavior pf cellulose nanoparticles during freeze drying: Effect pf suspension concentration, particle size, crystal structure and surface charge. *Biomacromolecules*, *14*, 1529–1540.

Kaewprasit, C., Hequet, N., Abidi, J. P., & Gourlot, J. (1998). Application of methylene blue adsorption to cotton fiber specific surface area measurement. Part I: Methodology. *Journal of Cotton Science*, *3*, 164–173.

Kvien, I., Tanem, B. S., & Oksman, K. (2005). Characterization of cellulose whiskers and its nanocomposite by atomic force and electron microscopy. *Biomacromolecules*, *6*, 3160–3165.

Li, N., & Bai, R. B. (2005). Copper adsorption on chitosan–cellulose hydrogel beads: Behaviors and mechanisms. *Separation and Purification Technology*, *42*, 237–247.

Li, N., Bai, R. B., & Liu, C. (2005). Enhanced and selective adsorption of mercury ions on chitosan beads grafted with polyacrylamide via surface-initiated atom transfer radical polymerization. *Langmuir*, *21*, 11780–11787.

Lin, Y. F., Chen, H. W., Chien, P. S., Chiou, C. S., & Liu, C. C. (2011). Application of bifunctional magnetic adsorbent to adsorb metal cations and anionic dyes in aqueous solution. *Journal of Hazardous Materials*, *185*, 1124–1130.

Liu, P., Sehaqui, H., Tingaut, P., Wichser, A., Oksman, K., & Mathew, A. P. (2014). Biobased nanomaterials for capturing silver ions (Ag+) from water via surface adsorption. *Cellulose*, *21*, 449–461.

Liu, C. C., Wang, M. K., & Li, Y. S. (2005). Removal of nickel from aqueous solution using wine processing waste sludge. *Industrial and Engineering Chemistry Research*, *44*, 1438–1445.

Ma, H., Burger, C., Hsiao, B. S., & Chu, B. (2011). Ultra-fine cellulose nanofibers: New nano-scale materials for water purification. *Journal of Materials Chemistry*, *21*, 7507–7510.

Ma, H., Burher, C., Hsiao, B. S., & Chu, B. (2011). Ultrafine polysaccharide nanofibrous membrane for water purification. *Biomacromolecules*, *12*, 970–976.

Ma, H., Burger, C., Hsiao, B. S., & Chu, B. (2012). Nanofibrous microfiltration membrane based on cellulose nanowhiskers. *Biomacromolecules*, *13*, 180–186.

Mathew, A. P., Laborie, M.-P., & Oksman, K. (2009). Cross-linked chitosan/chitin crystal nanocomposites with improved permeation selectivity and pH stability. *Biomacromolecules*, *10*, 1627–1632.

Mathew, A. P., Oksman, K., Pierron, D., & Harmand, M.-F. (2012). Fibrous cellulose nanocomposite scaffolds prepared by partial dissolution for potential use as ligament or tendon substitutes. *Carbohydrate Polymers*, *87*, 2291–2298.

Mikkonen, K. S., Mathew, A. P., Pirkkalainen, K., Serimaa, R., Xu, C., Willfor, S., et al. (2010). Glucomannan composite film with cellulose nanowhiskers. *Cellulose*, *17*, 69–81.

Min, M., Shen, L., Hong, G., Zhu, M., Zhang, Y., & Wang, X. (2012). Micro–nano structure poly(ether sulfones)/poly(ethyleneimine) nanofibrous affinity membrane for adsorbtion of anionic dyes and heavy metals ions in aqueous solution. *Chemical Engineering Journal*, *197*, 88–100.

Muzzarelli, R. A. A. (2012). Nanochitins and nanochitosans, paving the way to eco-friendly and energy-saving exploitation of marine resources. *Polymer Science: A Comprehensive Reference*, *10*, 153–164.

Muzzarelli, R. A. A., Morganti, P., Morganti, G., Palombo, P., Palombo, M., Biagini, G., et al. (2007). Chitin nanofibrils/chitosan glycolate composites as wound medicaments. *Carbohydrate Polymers*, *70*, 274–284.

Narges, N., Algan, C., Jacobs, V., John, M., Oksman, K., & Mathew, A. P. (2014). Electrospun chitosan-based nanocomposite mats reinforced with chitin nanocrystals for wound dressing. *Carbohydrate Polymers*, *109*, 7–15.

Pavia, D. L., Lampman, G. M., & Kriz, G. S. (2002). *Introduction to spectroscopy. A guide for students of organic chemistry*. Mexico: Thomson Learning.

Petersson, L., Kvien, I., & Oksman, K. (2007). Structure and thermal properties of poly(lactic acid)/cellulose whiskers nanocomposite materials. *Composites Science and Technology*, *67*, 2535–2544.

Samir, M. A., Alloin, F., & Dufresne, A. (2005). Review of recent research into cellulosic whiskers, their properties and their application in nanocomposites field. *Biomacromolecules*, *6*, 612–626.

Saxena, A., Elder, T. J., Pan, S., & Ragauskas, A. J. (2009). Novel nanocellulosic xylan composite film. *Composites: Part B*, *40*, 727–730.

Shigemasa, Y., Matsuura, H., Sashiwa, H., & Saimoto, H. (1996). Enzymatic degradation of chitins and partially deacetylated chitins. *International Journal of Biological Macromolecules*, *18*, 237–242.

Strand, S., Sauperl, O., & Fras-Zemljic, L. (2010). *Cellulose fibers functionalized by chitosan: Characterization and application*. In M. Elnashar (Ed.), *Biopolymer*. ISBN: 978-953-307-109

Wesenberg, D., Kyriakides, I., & Agathos, S. N. (2003). White-rot fungi and their enzymes for the treatment of industrial dye effluents. *Biotechnology Advances*, *22*, 161–187.

Xiao, S., Shen, M., Guo, R., Huang, Q., Wang, S., & Shi, X. (2010). Fabrication of multi-walled carbon nanotube-reinforced electrospun polymer nanofibers containing zero-valent iron nanoparticles for environmental applications. *Journal of Materials Chemistry*, *20*, 5700–5708.